In Fig. 4b, values of the skin friction coefficient are presented as a function of the Clauser integral shape parameter [5]:

$$G = \int_0^1 \left(\frac{u_\infty - u}{u_*}\right)^2 d(y/\delta) \Big/ \int_0^1 \left(\frac{u_\infty - u}{u_*}\right) d(y/\delta) = \left(\frac{2}{c_f}\right)^{1/2}\left(1 - \frac{1}{H}\right),$$

which is related to the shape of the velocity profile in the boundary layer. As is evident, the nonuniqueness develops less here than in Fig. 4a; it also appears worthwhile to construct the relation $c_f(G)$ instead of $\Psi(G)$.

## LITERATURE CITED


1. E. U. Repik, Inzh.-Fiz. Zh., 22, No. 3 (1972).
2. E. U. Repik, Tekh. Otchety Tsentr. Aero-Gidrodinam. Inst. im. N. E. Zhukovskii, No. 150 (1959).
3. N. I. Konstantinov and G. L. Dragnysh, Tr. Leningr. Politekh. Inst., No. 176 (1955).
4. D. A. Spence and G. L. Brown, J. Fluid Mech., 33, Part 4 (1968).
5. F. H. Clauser, J. Aeronaut. Sci., 21, No. 2 (1954).
6. D. Preston, in: Mekhanika [Period Collection of Translations of Foreign Articles], No. 6 (1955).
7. E. U. Repik, Tr. Tsentr. Aero-Gidrodinam. Inst., No. 1218 (1970).
8. V. Patel, J. Fluid Mech., 23, Part 1 (1965).
9. E. U. Repik and V. N. Tarasova, Tr. Tsentr. Aero-Gidrodinam. Inst. im. N. E. Zhukovskii, No. 1218 (1970).
10. H. Ludweig and W. Tillmann, TM 1285, NACA (1950).
11. M. R. Head and V. C. Patel, R and M 3643, ARC (1969).
12. V. I. Zimenkov, Inventor's Certificate No. 149919, Byul. Izobret., No. 17 (1962).
13. A. G. Taryshkin and V. V. Svirin, Author's Certificate 268680 (1969); Otk. Izobret., Prom. Obraz., Tovar. Znaki, No. 14 (1970).
14. S. Dhawen, TN 2567, NACA (1952).
15. B. Narayanan and V. Ramjee, J. Aeronaut. Soc. India, 20, No. 1 (1968).


# DETERMINATION OF THE DISTANCE TO A TURBULENT CONE DURING THE INTERACTION BETWEEN LAMINAR AXISYMMETRIC FREE JETS


V. N. Dmitriev and N. A. Kuleshova



UDC 532.517.3.001.5



Results are presented of an experimental investigation to determine the distance to the turbulent cone originating in a laminar feeding jet during its interaction with a laminar control jet.


Turbulent amplifiers [1, 2], whose operating principle is based on the forced turbulization of the axisymmetric free feeding submerged jet by a laminar control jet of the same type and on the deflection of the feeding jet, have recently been used extensively in jet pneumoautomation. In this connection, the question of determining the distance to the turbulent cone of the laminar feeding jet, which is needed for the computation of the static and dynamic characteristics of a turbulent amplifier, is urgent.

It is known that if mechanical obstacles, control jets, sound fields, etc., do not act on an axisymmetric laminar free jet, then the laminar jet becomes unstable for $Re_0 > 30$ [1], computed according to the stream in the capillary shaping the jet, and there is a transition to turbulence. The loss of the laminar jet stability is explained by vortex origination during its emergence from the capillary [3], which spoils the laminar structure by acting on the jet.


Moscow Automobile Road Institute.


Translated from Inzhenerno-Fizicheskii Zhurnal, Vol. 30, No. 5, pp. 803-810, May, 1976. Original article submitted March 3, 1975.

TABLE 1. Capillary Dimensions

| | [5] | | | | | [6] | | |
|---|---|---|---|---|---|---|---|---|
| $d_0$, mm | 0,88 | 0,805 | 0,65 | 0,76 | 1,17 | 1,21 | 2,37 | 1,21 |
| $l_0/d_0$ | 68,5 | 124 | 183 | 204 | 560 | 74,05 | 103,1 | 49,37 |

As the number $Re_0$ of the capillary increases, the turbulent cone approaches its exit. The dimensionless distance $x_{fe}/d_0$ from the exit of the capillary to the transition section depends mainly on the number $Re_0$ of the capillary. In addition, the location of the turbulent cone depends on such seemingly secondary factors as the condition of the entrance to the capillary, the presence of sound, and the weak motion of air. As has recently become known, the gas composition exerts an influence on the position of the turbulent cone. This property is used in the tube element – the tube to construct the sensors of gas analyzers [4].

Experimental data to determine the distance $x_{fe}$ during natural turbulization have been obtained [5] on the basis of inspecting five capillaries with different lengths and diameters. All the capillaries inspected had a 90° entrance edge. Room-temperature air was used as the gas. The effect of secondary perturbing effects was excluded in the experimental investigations.

The capillary dimensions are presented in Table 1.

All the experimental data have been plotted on graphs with the coordinates $x_{fe}/d_0 - Re_0$. Moreover, experimental data from [6], which agreed satisfactorily with our results obtained earlier and refined later, were also plotted on the same graphs. The experimental dependence obtained was approximated by the equation

$$\frac{x_{fe}}{d_0} = k\left(\frac{Re_{cr0}^2}{Re_0} - Re_0\right). \quad (1)$$

An equation has been obtained in [1] on the basis of using the theory of boundary-layer stability on a solid wall. By comparison with similar data presented in other papers [7, 8], where $x_{fe}/d_0 = f(Re_0)$ is represented by hyperbolic dependences, (1) corresponds most completely to the physical crux of the phenomenon of turbulent cone formation in a laminar jet. Indeed, for $Re_0 = Re_{cr\,0}$, $x_{fe} = 0$, i.e., the transition section agrees with the exit of the capillary. When $Re_0 \to 0$, then $x_{fe} \to \infty$, which is also verified experimentally. We obtained numerical values of the coefficients k and $Re_{cr\,0}$ by approximating the experimental curve mentioned by using (1). In conformity with this, (1) can be written as

$$\frac{x_{fe}}{d_0} = 3.32\cdot 10^{-3}\left(\frac{21.2\cdot 10^6}{Re_0} - Re_0\right). \quad (2)$$

The interaction diagram between a laminar feeding jet and a laminar control jet is shown in Fig. 1, where all the necessary parameters are denoted.

The intensity of the effect of the control jet on the feeding jet will be characterized by the ratio between the impulses $j = I_1/I_0$ of constant-mass control and feeding jets at the site of their collision, where $I_1$ is the impulse of the constant-mass control jet stream at the collision site, and $I_0$ is the analogous parameter of the feeding jet.

A constant-mass jet [1] is understood to be that part of the jet in which the discharge remains constant and equal to the discharge $Q_0$ passing through the escape hole. Namely, a constant-mass jet is seen in visualizing a laminar free and submerged jet, since the surrounding gas it ejects is transparent and there is no transverse mixing.

The ratio between the impulses $j = I_1/I_0$ corresponds to the tangent of the angle of deflection of the jet issuing from the feeding capillary, i.e., $j = \tan\varphi$. Formulas to determine j, obtained under the assumption of a constant gas density, are presented in [9]. The comparison presented in this paper between the experimental and calculated data, performed by using the formulas mentioned, exhibits good agreement.

The determination of the dimensionless distances between the endface of the feeding capillary and the transition section as a function of the ratio between the impulses $x_{fe}/d_0$ was accomplished on the basis of processing a large series of photographs on each of which a feeding jet deflected by a control jet was visualized by smoke. Three different pairs of feeding and control capillaries were examined. Their geometric dimensions are indicated in Table 2. The different feeding pressures $P_0$ were given for each pair of feeding and control capillaries, and their mutual location, characterized by the distances $x_t'$ and $x_{1t}'$ (see Table 2), varied.

TABLE 2. Dimensions of the Feeding and Control Capillaries, Their Relative Location, and the Feeding Pressure

| First pair of capillaries | | | | | Second pair of capillaries | | | | | Third pair of capillaries | | | | |
|---|---|---|---|---|---|---|---|---|---|---|---|---|---|---|
| $d_0$=0,97 mm, $\frac{l_0}{d_0}$=196<br>$d_1$=0,715 mm, $\frac{l_1}{d_1}$=56 | | | | | $d_0$=0,76 mm, $\frac{l_0}{d_0}$=92<br>$d_1$=0,515 mm, $\frac{l_1}{d_1}$=45 | | | | | $d_0$=0,835 mm, $\frac{l_0}{d_0}$=84<br>$d_1$=0,515 mm, $\frac{l_1}{d_1}$=45 | | | | |
| $P_0$, Pa | $Re_0$ | $x'_t$, mm | $\frac{x'_t}{x'_{1t}}$ | experimental points | $P_0$, Pa | $Re_0$ | $x'_t$, mm | $\frac{x'_t}{x'_{1t}}$ | experimental points | $P_0$, Pa | $Re_0$ | $x'_t$, mm | $\frac{x'_t}{x'_{1t}}$ | experimental points |
| | | 0,64 | 0,427 | *1* | | | 0,62 | 0,661 | *18* | | | 0,62 | 0,661 | *27* |
| | | 1,28 | 0,427 | *2* | 981 | 492 | 2,19 | 2,907 | *19* | 981 | 570 | 2,19 | 2,907 | *28* |
| 981 | 433 | 6,4 | 5 | *3* | | | 4,80 | 5,832 | *20* | | | 4,80 | 5,832 | *29* |
| | | 1,28 | 1 | *4* | | | 0,62 | 0,661 | *21* | | | 0,62 | 0,661 | *30* |
| | | 3 | 2,542 | *5* | 1962 | 894 | 2,19 | 2,907 | *22* | 1962 | 992 | 2,19 | 2,907 | *31* |
| 1471 | 639 | 0,64 | 0,427 | *6* | | | 4,80 | 5,832 | *23* | | | 4,80 | 5,832 | *32* |
| | | 0,64 | 0,427 | *7* | | | 0,62 | 0,661 | *24* | | | 0,62 | 0,661 | *33* |
| | | 1,28 | 0,427 | *8* | 2943 | 1212 | 2,19 | 2,907 | *25* | 2943 | 1317 | 2,19 | 2,907 | *34* |
| 1962 | 829 | 6,4 | 5 | *9* | | | 4,80 | 5,832 | *26* | | | 4,80 | 5,832 | *35* |
| | | 1,28 | 1 | *10* | | | | | | | | | | |
| | | 3 | 2,542 | *11* | | | | | | | | | | |
| | | 0,64 | 0,427 | *12* | | | | | | | | | | |
| | | 1,28 | 0,427 | *13* | | | | | | | | | | |
| 2943 | 1164 | 6,4 | 5 | *14* | | | | | | | | | | |
| | | 1,28 | 1 | *15* | | | | | | | | | | |
| | | 3 | 2,542 | *16* | | | | | | | | | | |
| 3924 | 1458 | 0,64 | 0,427 | *17* | | | | | | | | | | |

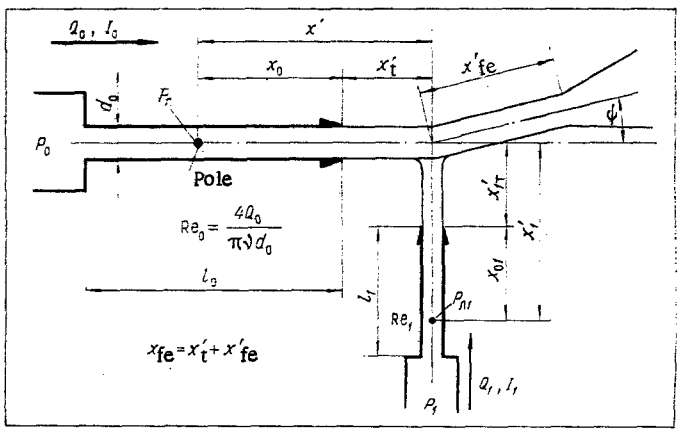


Fig. 1. Diagram of interaction between laminar feeding and laminar control jets.

The tangent of the angle of jet rotation $\tan \psi = I_1 / I_0 = j$ and the distance $x_{fe} / d_0$ were determined for each of the combinations indicated in Table 2 during processing of the photographs. Moreover, an analysis of the photographs permitted setting up a number of qualitative phenomena originating during laminar jet collisions. One of them is that the laminar control jet does not mix with the laminar feeding jet in the collision zone but flows around it as a solid cylinder. This phenomenon was also fixed earlier by a number of other researchers ([10], for example). Only when the turbulent cone enters the zone of jet interaction does intensive mixing start. A second phenomenon appears in the "waisting" below of the feeding jet by the control jet, which results in distortion of the longitudinal velocity profile of the feeding jet near the collision zone. The angles of deflection $\psi$ of the feeding jet reach significant values in some cases. Thus, when the transition section approaches the intersection of the capillary axes ($x_{fe} = x'_t$), the angle has its greatest value equal to approximately 30° for some pairs of control and feeding capillaries used in practice. In this connection, the turbulent amplifier characteristics must be computed taking into account the angle of deflection of the feeding jet. Otherwise, significant errors can occur.

For $j = 0$ the turbulent cone is formed because of natural turbulization and the distance thereto is determined by the dependence (2). An increase in $j = I_1 / I_0$ results in a diminution in $x_{fe} / d_0$, and for a definite critical value of the ratio between the stream impulses $j_{cr}$, the dimensionless distance to the cone $x_{fe} / d_0$ becomes

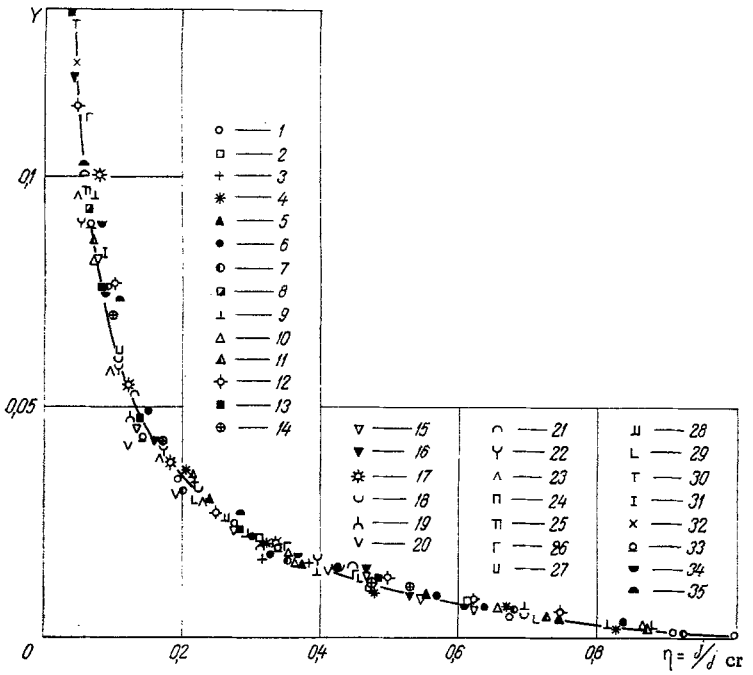


Fig. 2. Normalized dependence of the dimensionless distance between the intersection of the capillary axes and the transition section on the dimensionless impulse. See Table 2 for the values 1-35. The solid curve is according to (3).

equal to the dimensionless distance $x_t'/d_0$. A further increase in j above the critical value no longer causes a change in $x_{fe}/d_0$, since the turbulent cone cannot be moved upstream in the jet. In order to determine the quantity $j_{cr}$ by means of data from an experiment obtained because of processing the photographs mentioned, curves characterizing the dependence of the dimensionless distance $x_{fe}/d_0$ on the ratio between the impulses of constant-mass streams $j = I_1/I_0$ were constructed. Each family of curves corresponded to a definite pair of feeding and control capillaries and their fixed mutual arrangement and each curve of the family, to a definite $Re_0$. The value of $j_{cr}$ was determined by the abscissa of the intersection between the curve and the line $x_{fe}/d_0 = x_t'/d_0 = \text{const}$. The mentioned curves permit seeking the distance $x_{fe}/d_0 = (x_t'/d_0) + (x_{fe}'/d_0)$ according to a given geometry for the control and feeding capillaries, their Reynolds numbers, and their mutual disposition. However, it is very complicated to use a whole series of such graphs, and, moreover, they are effective only for some particular cases. Hence, a generalized normalized curve was constructed in similarity criteria on the basis of the test data obtained, which affords the possibility of determining the distance $x_{fe}/d_0$ for any pair of capillaries, their mutual arrangement, and their Reynolds numbers (Fig. 2). Plotted along the vertical axis is the ratio between the distance from the intersection of the capillary axes to the transition section and this same distance, but in the absence of a control signal, while the ratio between the dimensionless stream impulse $j = I_1/I_0$ and its critical value $j_{cr} = (I_1/I_0)_{cr}$ is plotted along the horizontal. Therefore, when the dimensionless distance along the vertical axis is zero, the corresponding ratio between the dimensionless impulses $\eta = j/j_{cr}$ equals one on the horizontal axis. When the ratio between the dimensionless impulses equals zero, then the dimensionless distance equals one. The dependence approximating the curve (Fig. 2) is

$$Y = A\left(\frac{1+B}{\eta+B} - \eta\right), \tag{3}$$

where

$$Y = \frac{\frac{x_{fe}}{d_0} - \frac{x_t'}{d_0}}{k\left(\frac{Re_{cr\,0}^2}{Re_0} - Re_0\right) - \frac{x_t'}{d_0}};$$

$k = 3.32 \cdot 10^{-3}$; $Re_{cr\,0}^2 = 21.2 \cdot 10^6$; $A = 7.5 \cdot 10^{-3}$; $B = 0.0076$; $\eta = j/j_{cr}$. The ratio between the impulses $j = \tan\psi$ can be computed by means of formulas presented in [9]. For the most widespread case $x_t' \leq 0.0375 Re_0 d_0$ and $x_{1t}' \leq 0.0375 Re_1 d_1$, this dependence is

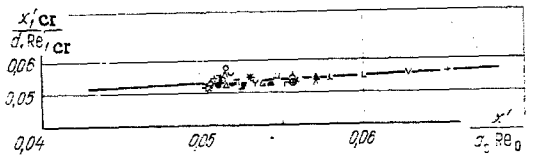


Fig. 3

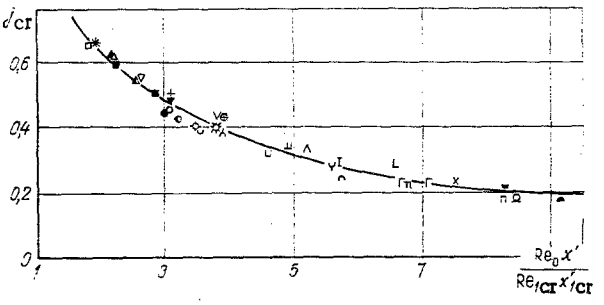


Fig. 4

Fig. 3. Dependence of the reduced distance $x'_{1cr}/d_1Re_{1cr}$ on the reduced distance $x'/d_0Re_0$.

Fig. 4. Dependence of the dimensionless stream impulse $j_{cr}$ on the dimensionless complex $Re_0 \cdot x'/Re_{1cr}x'_{1cr}$.

$$j = \left(\frac{Re_1}{Re_0}\right)^2 \frac{1-\left(0.3+\dfrac{4x'_1}{Re_1 d_1}\right)^3}{1-\left(0.3+\dfrac{4x'}{Re_0 d_0}\right)^3},$$

where $x' = x_0 + x'_t$, $x'_1 = x_{01} + x'_{1t}$. The quantities x and $x_{01}$ are the distances between the capillary exit and the provisional source $P_p$ and $P_{p1}$, respectively, and are expressed by the known dependences [11]

$$x_0 = 0.05Re_0 d_0; \quad x_{01} = 0.05Re_1 d_1.$$

Two graphs (Figs. 3 and 4) were constructed according to the experimental data in order to seek $j_{cr}$. In order to find $j_{cr}$, the $x'/d_0Re_0$ is computed and the $x'_{1cr}/d_1Re_{1cr}$ is found from the curve in Fig. 3. Then starting from the dependence

$$\frac{x'_{1t}}{d_1 Re_{1cr}} + 0.05 = \frac{x'_{1cr}}{d_1 Re_{1cr}},$$

the $Re_{1cr}$ is found and

$$\frac{Re_0 x'}{Re_{1cr} x'_{1cr}} = \frac{Re_0 (0.05Re_0 d_0 + x'_t)}{Re_{1cr}(0.05Re_{1cr} d_1 + x'_{1t})}$$

is computed. After this, the $j_{cr}$ is sought from Fig. 4. Here the Reynolds number $Re_{cr}$ and distance $x'_{1cr}$ from the pole $P_{p1}$ of the control capillary to the feeding capillary axis correspond to the critical ratio between the impulses $j_{cr}$.

## NOTATION

$Re_0$, feeding capillary Reynolds number; $x_{fe}$, distance between the feeding capillary endface and the transition section, mm; $d_0$, feeding capillary diameter, mm; k, constant factor; j, ratio between dimensionless constant-mass jet impulses at the collision site; $I_1$, $I_0$, constant-mass control and feeding jet stream impulses at the collision site, kgm/sec$^2$; $\varphi$, angle of feeding jet deflection; $P_0$, feeding pressure, Pa; $x'_t$, $x'_{1t}$, distances between the feeding and control capillary endfaces and the intersection of the capillary axes, respectively, mm; $j_{cr}$, critical ratio between the impulses corresponding to the coincidence of the transition section with the intersection of the capillary axes; A, B, constant coefficients; $\eta = j/j_{cr}$, ratio between dimensionless impulses; $Re_1$, Reynolds number of the control capillary; $x'_1$, distance between the control capillary pole $P_{p1}$ at the point of intersection of the capillary axes, mm; x', distance from the pole $P_p$ of the feeding capillary to the intersection of the capillary axes, mm; $x_0$, $x_{01}$, pole distance of the feeding and control capillaries, mm; $Re_{1cr}$, critical Reynolds number of the control capillary, corresponding to coincidence between the transition section and the intersection of the capillary axes.

## LITERATURE CITED

1. I. V. Lebedev, S. L. Treskunov, and V. S. Yakovenko, Elements of Jet Automation [in Russian], Mashinostroenie, Moscow (1973).
2. L. A. Zalmanzon and I. V. Lebedev (editors), Jet Techniques. Transactions of the Jablonski Conference [Russian translation], Mir, Moscow (1969).

3. Abramowitz and Solan, in: Dynamic Systems and Control. Series G [Russian translation], No. 2 (1973).
4. R. Sh. Perlovskii, Automation of Chemical Production [in Russian], No. 1, Moscow (1969), p. 111.
5. V. G. Gradetskii and V. N. Dmitriev, Prib. Sist. Upravl., No. 2 (1967).
6. Bell, in: Dynamic Systems and Control. Series G [Russian translation], No. 2 (1973).
7. L. A. Vulis, V. G. Zhivov, and L. P. Yarin, Inzh.-Fiz. Zh., 17, No. 2 (1969).
8. V. I. Ashikhmin, Izv. Vyssh. Uchebn. Zaved., Neft' Gaz, No. 6 (1967).
9. V. N. Dmitriev, N. A. Kuleshova, and Yu. D. Vlasov, in: Transactions of the Moscow Automobile Road Institute. Hydropneumoautomation and Hydraulic Drives [in Russian], No. 74, Moscow (1974), p. 139.
10. E. Dexter, in: Jet Pneumohydroautomation [Russian translation], Mir, Moscow (1966), p. 300.
11. E. N. Andrade and L. C. Tsin, Proc. Physical Soc., 49, 381-391 (1937).

# METHODS OF INVESTIGATING THE SOLVABILITY OF SYSTEMS OF LINEAR EQUATIONS OF THERMOANEMOMETRY

M. Hoffmeister and G. Seifert

UDC 532.57

Use of thermoanemometry for the investigation of turbulent flows often leads to systems of linear equations that are difficult to solve. A numerical method of solution, in which measurement errors are taken into account approximately, is proposed for the investigation of solvability of such systems of equations.

As we know, the heat emission from a heated filament to its surrounding medium depends on the modulus and direction of the vector of the velocity relative to the filament, as well as on the temperature of the filament and the medium. For sufficiently small velocities of the flow it depends on the orientation of the filament in the field of the force of gravity and to a small degree on the construction of the probe and the static pressure of the medium (see, for example, [1-4]). The value of the electric voltage at the output of the thermoanemometer characterizes the heat exchange of the filament and therefore, as a rule, is a function of several parameters corresponding to the cases mentioned above. When carrying out and processing measurements we first and foremost pursue the objective by means of different methods of measurement – for example, using multifilament transducers or successively carrying out measurements with different positions of the filament in a stationary flow – to obtain a system of equations which is solvable relative to the individual parameters of flow that are of interest to us.

The present work contains analytical investigations on the basis of the so-called cosine law [1] and investigations by the least squares method [5-8] of the matrices of systems of linear equations of thermoanemometry. Separate consideration is given to the methods of measuring with a single-filament transducer to determine the average velocity vector and Reynolds stresses in stationary turbulent flows which in the general case are three-dimensional. It is assumed that the fluid is Newtonian, isothermal, homogeneous, and incompressible. The basic propositions of these investigations are presented in [9-12] and will be repeated here to the extent which is necessary for the understanding of the present work.

## 1. Application of the "Cosine Law"

A quadratic approximation of the three-dimensional calibration characteristic of the probe according to [11] leads to the following relation between the single-point moments of the velocity field and the output voltage of the thermoanemometer:

$$\left(\hat{a}_i + \hat{b}_{ij}\,\frac{\Delta\hat{w}_j}{\hat{c}}\right)\frac{\Delta\hat{w}_i}{\hat{c}} + \hat{b}_{ij}\,\frac{\overline{w_i' w_j'}}{\hat{c}^2} = \Delta F \quad (i, j = 1, 2, 3), \tag{1}$$

Academy of Sciences of the German Democratic Republic, Berlin. Translated from Inzhenerno-Fizicheskii Zhurnal, Vol. 30, No. 5, pp. 811-820, May, 1976. Original article submitted April 15, 1975.